Supporting Information Corrected November 21, 2016

Supplemental material for the paper

EVOLUTIONARY ALTERATION OF ALOX15 SPECIFICITY IS AIMED AT OPTIMIZING THE BIOSYNTHESIS OF ANTI-INFLAMMATORY LIPOXINS

Susan Adel[1], Felix Karst[1], Àngels González-Lafont[2,3], Mária Pekárová[1,4], Patricia Saura[2,3], Laura Masgrau[3], José M. Lluch[2,3], Sabine Stehling[1], Thomas Horn[1,5], Hartmut Kühn[1*], Dagmar Heydeck[1]

[1]Institute of Biochemistry, University Medicine Berlin - Charité, Charitéplatz 1, CCO-Building, Virchowweg 6, D-10117 Berlin, Germany; [2]Departament de Química and [3]Institut de Biotecnologia i de Biomedicina (IBB), Universitat Autònoma de Barcelona, 08193 Bellaterra, Barcelona, Spain; [4]Department of Cell and Molecular Biology of Drugs, Faculty of Pharmacy, Comenius University, Kalinčiakova 8, 832 32 Bratislava, Slovakia

[5]present affiliation: Institut für Biotechnologie, Rheinisch-Westfälische Technische Hochschule Aachen, Worringer Weg 3, 52074 Aachen, Germany

1. Additional methodological information

Chemicals - The chemicals used were obtained from the following sources: Arachidonic acid (5Z,8Z,11Z,14Z-eicosatetraenoic acid) from Sigma (Deisenhofen, Germany), HPLC standards of 5S-HETE, 8S-HETE, 12S-HETE, 12(±)-HETE, 15S-HETE, and 15(±)-HETE, 5S,15S-DiHETE, 8S,15S-DiHETE, 5S,6S-DiHETE, 5S,6R-DiHETE, lipoxin A4 (LxA4) and lipoxin B4 (LxB4) from Cayman Chem., Ann Arbor, USA (distributed by Biomol GmbH, Hamburg, Germany), sodium borohydride from Serva (Heidelberg, Germany), ampicillin, kanamycin and isopropyl-b-thiogalactopyranoside (IPTG) from Carl Roth (Karlsruhe, Germany). HPLC solvents were purchased from Merck (Darmstadt, Germany). Restriction enzymes were obtained from Thermo Scientific/Fermentas (Dreieich, Germany). Oligonucleotide synthesis was performed at BioTez (Berlin, Germany) and nucleotide sequencing was carried out at Eurofins MWG Operon (Ebersberg, Germany). The *E. coli* strains BL21(DE)pLysS and Rosetta2(DE3)pLysS were purchased from Agilent Technologies (Waldbronn, Germany).

PCR cloning of selected ALOX15 orthologs - To get the cDNA total RNA was first extracted from the blood of the animals using the blood RNA extraction kit from Qiagen. Next, the total RNA was reversely transcribed using Premium Reverse Transcriptase from Thermo Scientific/Fermentas and the ALOX15 cDNA was selectively amplified by PCR employing specific primers (forward primer 5'-CCC C**GT CGA C**AT GGG TCT CTA CCG C-3', reverse primer 5'-CCC C**AA GCT T**TT AGA TGG CCA CAC TGT T-3') and using Advantage PCR Mix (Takara Bio Europe/Clontec h, Saint-Germain-en-Laye, France). The forward primer contained a SalI and the reverse primer a HindIII restriction site (bold face) for convenient cloning into the expression vector. For initial amplification and modification the PCR fragment was first inserted into the TOPO 2.1 cloning vector (Life Technologies, Darmstadt, Germany) and internal HindIII sites were removed by silent site-directed mutagenesis. The final construct was then excised by SalI-HindIII digestion and the restriction fragment was inserted into the linearized prokaryotic expression vector pET28b. This construct was completely sequenced to ensure the absence of subcloning artifacts.

Bacterial expression of ALOX15 orthologs - For bacterial expression of ALOX15 orthologs competent bacteria [BL21(DE3)pLysS] or [Rosetta2(DE3)pLysS] were transformed with the recombinant pET28b expression plasmids and bacterial expression of the recombinant ALOX15 isoforms was carried out in 50 ml cultures using the optimized EnPresso-Expression system (BioSilta Oy, Oulu, Finland) following the instruction of the vendor. After the induction period the bacteria were pelleted, washed and resuspended in 4 ml PBS. Cells were disrupted by sonication (tip sonifier), debris were spun down and the clear lysis supernatant was used as enzyme source for direct activity assay.

Eucaryotic expression of P. anubis ALOX15 – Because of unknown reasons the *P. anubis* ALOX15 was only low level expressed in *E. coli* so that reliable activity assays were not possible. To overcome this problem we expressed the enzyme in murine neuroblastoma cells Neuro-2a (N2a) (LGC Standards GmbH, Wesel, Germany). For this purpose the coding region was excised from the pET 28b (+) procaryotic expression plasmid using the unique Xba I and Not I cloning sites. The restriction fragment containing the starting methionine and the his-tag epitope was then ligated into the pcDNA 3.1(-) eucaryotic expression vector and the recombinant plasmid was amplified in *E. coli XL-1 Blue competent cells*. For transfection, N2a cells were resuspended at a density of about 10^5 cells per ml in DMEM medium (4,5 g/l glucose, L-glutamine, 1mM sodium pyruvate, 3,7 g/l $NaHCO_3$ containing 10% fetal calf serum) and 2 ml of this suspension were seeded into each well of a 6-well plate (Sarstedt, Nümbrecht, Germany). Cells were allowed to attach for 24 h prior to transfection. Cell transfection was performed using the TransIT-LT1 transfection kit (Mirus bio, Madison, USA). For this purpose 2 µg of plasmid DNA were mixed with 6 µl TransIT-LT1 in 200 µl OptiMEM (Life Technologies, Inc., Eggenstein, Germany) and transfection complexes were allowed to form according to the manufacturer's protocol. Then the transfection mixture was added to each well and the cells were incubated with the transfection mixture at 37°C and 5% CO_2. After 48 h the cells were washed with PBS, harvested by resuspending, spun down (350 rpm for 3min) and the cell pellet was reconstituted in 0.5 ml of PBS. Next, cells were disrupted by sonifying the suspension twice for 10 s at 100% amplitude using an UP50H tip sonifier (Hielscher Ultrasound Technology, Teltow, Germany). Cell debris were spun down (16,000 rpm, 20 min, 4°C) and the lysis supernatant was used for activity assays, protein quantification and SDS-PAGE.

2. Sequence comparison of mammalian ALOX15 orthologs

Genes encoding for ALOX15 orthologs occur in all mammalian species sequenced so far. We extracted the cDNA sequences of mammalian ALOX15 orthologs of a large number of mammals from the publically available sequence databases and aligned the deduced amino acid sequences with that of the human enzyme. On the basis of these sequence data we calculated the degree of amino acid identity and these data are presented in **Table S1**. Compared to the human enzyme, the degree of strict amino acid conservation (amino acid identity) among mammalian ALOX15 orthologs ranges between 99.7 % (chimpanzee) and 61 % (cat). As expected, for species, which are closely related to humans (chimpanzee, *Pan troglodytes*) a high degree of amino acid identity was observed. Species, which are evolutionary more distant from humans, exhibit a lower degree of amino acid identity. Interestingly, the ALOX15 orthologs of lower mammals (opossum, wallaby) also exhibit high degrees of amino acid conservation (62% and 80% respectively). It should, however, been stressed that most of the mammalian ALOX15 orthologs have not been expressed and thus, it remains to be explored whether the enzymes are functional.

Table S1. Degree of amino acid identity of selected mammalian ALOX15 orthologs with human ALOX15.

Mammalian species	Amino acid homology (%)
H. sapiens	100
H. neanderthalensis	99.7
H. denisovan	99,7
Pan troglodytes	99.7
Gorilla gorilla	98.9
Pongo pygmeus	98.6
Macaca mulatta	94.6
Papio anubis	94.7
Saimiri boliviensis	88.2
Callithrix jaccus	86.8
Otolemur garnettii	88.4
Mus musculus	73.5
Rattus norvegicus	74.4
Cavia porcellus	64.9
Oryctolagus cuniculus (15-LOX)	81.0
Oryctolagus cuniculus (12-LOX)	81.0
Spermophilus tridecemlineatus	79.4
Felis catus	60.8
Sus scrofa	86.1
Bos taurus	76.4
Ceratotherium simum	89.5
Canis lupus familiaris	84.0
Mustela putorius furo	79.3
Ailuropoda melanoleuca	86.9
Sorex araneus	81.3
Loxodonta africana	86.1
Dasypus novemcinctus	89.0
Monodelphis domestica (Opossum)	61.7
Macropus eugenii (Wallaby)	69.9

2. Lipoxin formation of ALOX15 orthologs

To compare the capacity of ALOX15 orthologs for *in vitro* lipoxin formation we incubated aliquots of the different enzyme preparations exhibiting similar arachidonic acid oxygenase activities with 5S-HETE and with a 1:1 mixture of 5S,6S-DiHETE and 5S,6R-DiHETE. After reduction of the primary oxygenation products we analyzed them by RP-HPLC (see Materials and Methods) with a solvent system separating the lipoxin A4 (LxA4) and lipoxin B4 (LxB4) isomers. The products were analyzed by RP-HPLC using a Nucleosil C18 column (Marcherey-Nagel, Düren, Germany; KS-system, 250 x 4 mm, 5 µm particle size) coupled with a guard column (30 x 4 mm, 5-µm particle size) and the solvent system acetonitrile/water/acetic acid (38/62/0.1, by vol) at a flow rate of 1 ml/min. In **Fig. S1, A+B** the elution profile of commercial standards (Cayman Chem., Ann Arbor, USA) of LxA4 and LxB4 isomers are shown. It can bee seen that several isomers of conjugated tetraenes were present in the reference mixtures but all of them carried the characteristic conjugated tetraene chromophore. These isomers most probably originated from the pure standards by isomerization during long-term storage. Moreover example chromatograms for the formation of lipoxin isomers from 5S,6R/S-DiHETE by human **(Fig. S1, C)** and mouse **(Fig. S1, D)** are shown. The selected chromatograms indicate that the amounts of conjugated tetraenes formed by the human enzyme was much higher than that formed by mouse Alox15. **Fig. S1, E** indicates the uv-spectra of the conjugated tetraenes formed by human ALOX15 taken during the chromatographic run at the time points indicated by a, b and c

(Fig. S1, C). It can be seen that a mixture of different conjugated tetraenes was formed (Fig. S1, C) but all these isomers carry the conjugated tetraene chromophore.

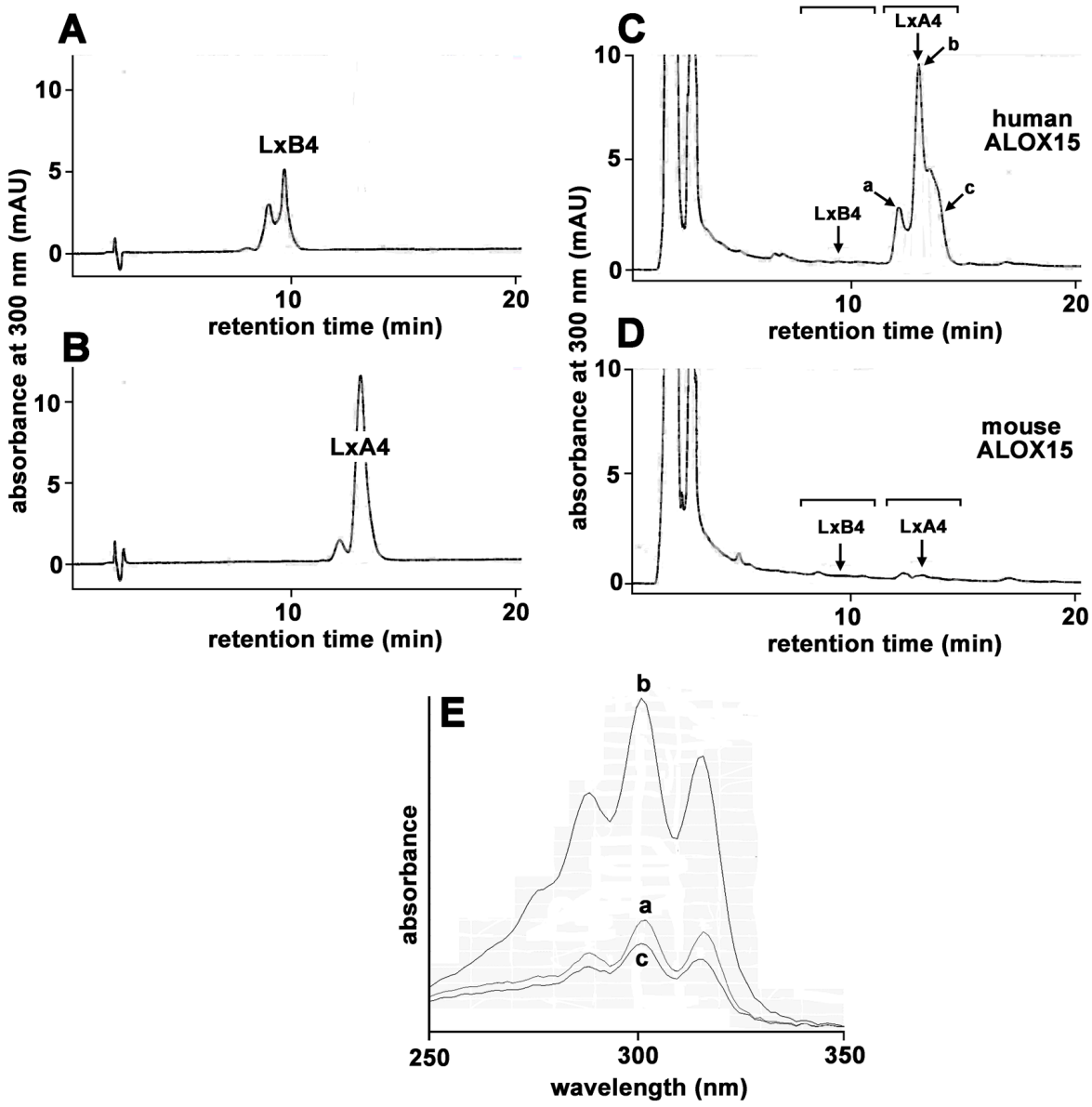

Fig. S1. Lipoxin synthase activity of mammalian ALOPX15 orthologs. Lipoxin synthase activity assays of the crude enzyme preparations were carried out as described in Materials and Methods. A) Authentic standard of LxB4. B) Authentic standard of LxA4. C) Lipoxin synthase activity of human ALOX15 (5S,6S/R-DiHETE as substrate). D) lipoxin synthase activity of mouse Alox15 (5S,6S/R-DiHETE as substrate). For quantification of the lipoxin synthase activities of the different mammalian ALOX15 orthologs all peaks absorbing at 300 nm in the appropriate time range (indicated by the signs above the chromatographic traces) were integrated. E) Comparison of uv-spectra of the lipoxin isomers formed from 5S-HETE by human ALOX15.

3. Sequence comparison of ALOX15B orthologs

In contrast to human ALOX15B, which converts arachidonic acid almost exclusively to 15-HpETE, the mouse ortholog (Alox15b) produces mainly 8-HpETE. The molecular basis for the different reaction specificities of these two enzymes has been explored **(1)** and two critical amino acids have been identified. To explore whether the different reaction specificities of these two enzyme orthologs are also a consequence of a targeted

evolutionary process, we compared the amino acids occupying these positions in different mammalian ALOX15B orthologs **(Table S2)** and found that, except for mice, the other orthologs carry amino acids, which are similar to those of the human enzyme. Thus, the reaction specificity of these orthologs should be similar to the human enzyme (15-lipoxygenating). Only the mouse enzyme carries the determinants responsible for arachidonic acid 8-oxygenation. Even rat ALOX15B, which is most similar to the mouse ortholog, exhibits arachidonic acid 15-lipoxygenating activities as concluded from the sequence data.

Table S2. Sequence determinants for the reaction specificity of ALOX15B orthologs. The amino acid sequences of the different ALOX15B orthologs were aligned with the human enzyme. The amino acids aligning with the human residues 603 and 604 (Jisaka determinants) were extracted and summarized in Table S2. The one letter amino acid code was used.

Species	determinant 1 (AA 603)	Determinant 2 (AA 604)
Human	D	V
Chimpanzee	D	I
Orangutan	D	V
Rhesus monkey	D	V
Baboon	D	V
Pig	D	V
Rat	D	V
Mouse	Y	H

4. Computational Methods

In Silico Mutagenesis - The starting coordinates of the ALOX15-AA complex used in the present study were taken from a previous QM/MM simulation **(2)**. In particular, the minimum energy structure named XI **(2)** was taken to generate the initial coordinates of the *in silico* Ile418Ala ALOX15-AA mutant by changing the residue Ile418 to Ala with the Mutator Plugin of the VMD program **(3)**.

MD Simulations - The Molecular Dynamics (MD) protocol applied to generate molecular configurations of the Michaelis complex of the Ile418Ala ALOX15-AA mutant is described next. First, the system was fully solvated in an orthorhombic box of pre-equilibrated TIP3P water molecules, with dimensions of 125 Å x 79 Å x 85 Å. Seven sodium cations were added to neutralize the total charge of the system. The resulting system contains nearly 75500 atoms, with about 10600 of them belonging to the protein. Firstly, the system was submitted to some MM minimization steps and then, MD simulations under periodic boundary conditions (PBC) were started. The system was gradually heated from 25K to 300K during 80 ps, followed by an equilibration step of 200 ps at 300 K. During the heating steps, harmonic restraints were applied to the protein, which was gradually released, while ligand (and water molecules) was kept free of restraints. Finally, a production step of 5 ns was performed. Three different trajectories of 5 ns of production were run for each 15rLO mutant. The MD simulations were done at constant pressure and temperature (CPT) using the extended system constant pressure and the Hoover constant temperature algorithms **(4)**. A time step of 2 fs was used for the production steps. All of the bonds and angles involving hydrogen atoms were constrained by the SHAKE algorithm **(5)**. PBCs were built with the CRYSTAL facility of CHARMM **(6, 7)** using an orthorhombic cell unit. For long-range electrostatic, the Particle Mesh Ewald was used. All MD simulations were run with CHARMM version c35-b1. The force field topology and parameters for AA were derived from the CHARMM27 **(8, 9)** ones. CHARMM22 **(10, 11)** force field was used for protein atoms, but Fe and its first coordination sphere, for which were used the parameter

specifically derived by Saam el al. **(12)** Structural analysis of the simulations was performed with the CORREL module of CHARMM.

QM/MM Calculations - The QM/MM calculations have been carried out with the modular program package ChemShell **(13)** TURBOMOLE **(14)** has been employed for the DFT calculations, and the CHARMM22 and CHARMM27 force fields for the MM calculations using the DL_POLY **(15)** module in ChemShell. The interaction between the QM and the MM subsystems has been treated by an electronic embedding scheme **(16)** and a link atom scheme has been adopted to describe the QM/MM boundary, using the charge shift model. No cutoffs were introduced for the nonbonding MM and QM/MM interactions **(17)** QM/MM optimizations were performed employing the Limited-memory Broyden-Fletcher-Goldfard-Shanno (L-BFGS) algorithm **(18, 19)** for energy minimizations, and the microiterative optimizer, combining both the partitioned rational function optimizer (P-RFO) **(20, 21)** and the L-BFGS, during the transition state searches. These algorithms are implemented in the HDLCopt (Hybrid Delocalized Internal Coordinate Scheme) **(22)** module of Chemshell. In all calculations the QM subsystem has been described by the B3LYP hybrid functional **(23)** and the 6-31G(d) Pople basis set **(24)** has been used for C, H, O and N atoms, and the LANL2DZ basis set **(25)** for Fe. The QM region, which includes 74 atoms (link atoms not included), is comprised by 24 atoms of the lipid substrate, 11 atoms of each of the four His residues in the Fe coordination sphere (His361, His366, His541 and His545), 3 atoms of the terminal residue 663 in the coordination sphere, and the Fe(III)-OH-cofactor, able to accept the hydrogen from AA. Seven link atoms were used, five along the bonds Cα – QM atom of the five residues in the Fe coordination sphere, and two bonded to the aliphatic carbons of the lipid substrate (placed between C6-C7 and C16-C17). An averaging procedure **(26)** has been applied to calculate the average potential energy barrier corresponding to a set of *n* potential energy barriers according to the below equation. Here *R* is the gas constant, *T* is the temperature and is the potential energy barrier *i*.

$$\Delta E_{AV}^{\ddagger} = -RT\ ln\left\{\frac{1}{n}\sum_{i=1}^{n} exp\left(-\frac{\Delta E_i^{\ddagger}}{RT}\right)\right\}$$

5. **Computational results**

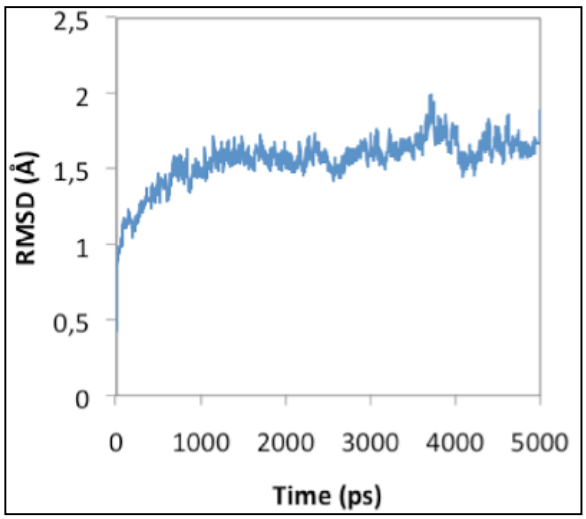

Figure S1. Protein RMSD (without H atoms) versus time for TRJ1

Given the flexibility observed for the ALOX15 enzyme in the available crystal structures and in the MD simulations carried out previously for the WT ALOX15-AA complexes, we decided to perform the conformational exploration of the Ile418Ala ALOX15-AA mutant system by running three non-correlated 5 ns simulations each one initiated with a slightly different protocol. Those three simulations are referred here as trajectory 1 (TRJ1), trajectory 2 (TRJ2) and trajectory 3 (TRJ3). The Root Mean Square Deviations (RMSDs) of the protein (without H atoms) along TRJ1, TRJ2 and TRJ3 with respect to the initial structures of those three 5 ns trajectories are shown in **Figures S1-S3**.

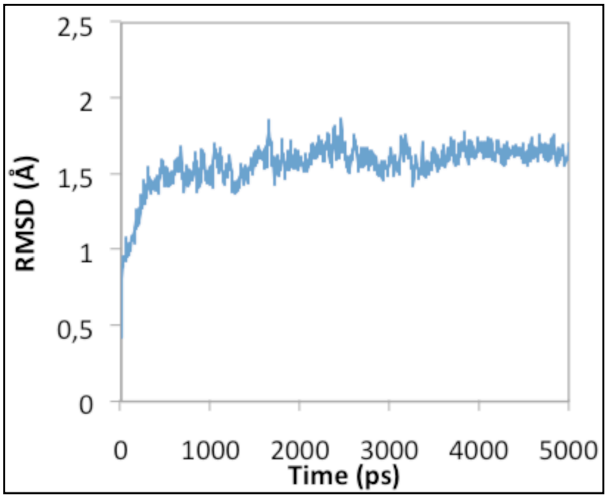

Figure S2. Protein RMSD (without H atoms) versus time for TRJ2

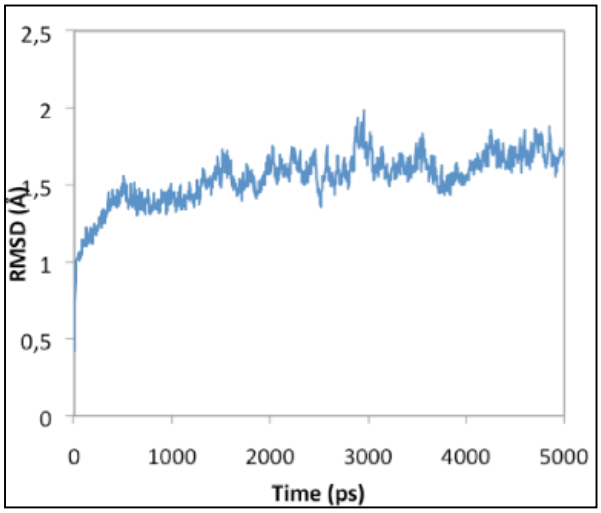

Figure S3. Protein RMSD (without H atoms) versus time for TRJ3

It can be observed that the three RMSDs with respect to the initial structure level off at a value around 1.5 Å, so indicating that the protein in the Ile418Ala ALOX15-AA mutant systems has relaxed to a more stable structure. The RMSDs of the heavy atoms of AA with respect to the substrate average structure again along TRJ1, TRJ2 and TRJ3 are shown in **Figures S4-S6**. The average RMSDs values for AA along TRJ1 and TRJ2 are very similar: 1.10 (0.46) Å and 1.13 (0.45) Å, respectively (standard deviation in parentheses). In both trajectories, however, there is a peak in the RMSDs evolution reflecting a clear reorientation of the AA molecule during a certain period of the simulation. The average RMSD for AA

along TRJ3 is greater (1.78 (0.56) Å) because the substrate changes its configuration more frequently in this third simulation.

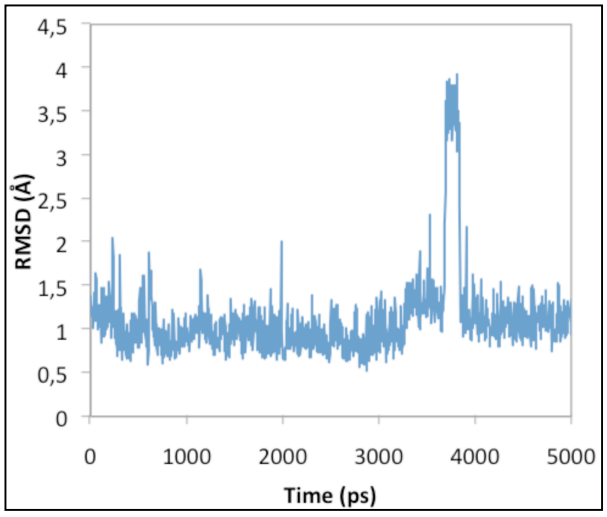

Figure S4. RMSD of the AA heavy atoms with respect to the average structure along TRJ1

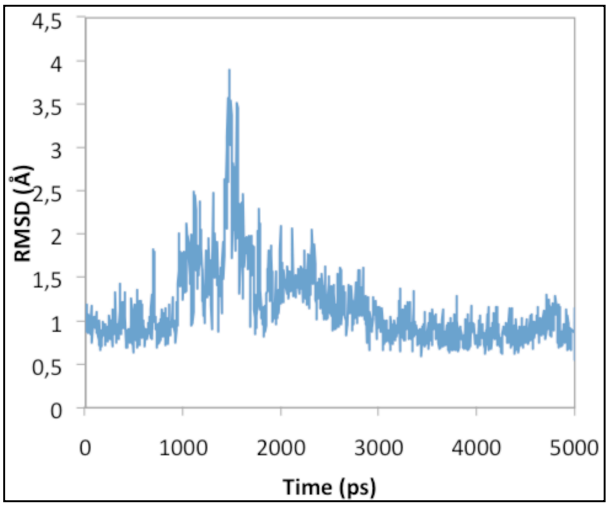

Figure S5. RMSD of the AA heavy atoms with respect to the average structure along TRJ2

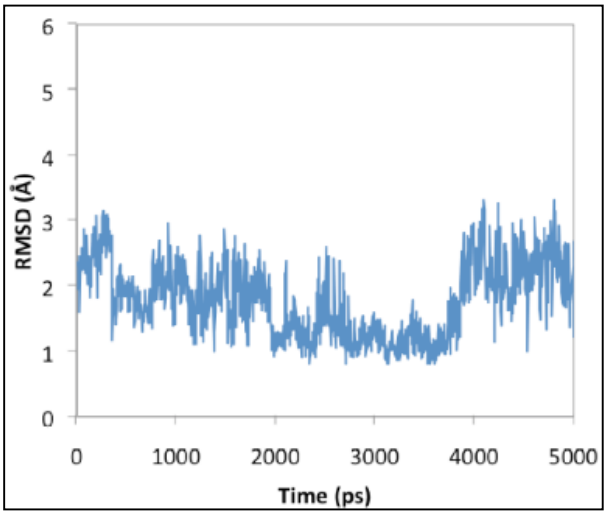

Figure S6. RMSD of the AA heavy atoms with respect to the average structure along TRJ3

Geometric parameter	TRJ1	TRJ2	TRJ3
$d(C_{13}\text{-OH})$	5.82 (0.61)	6.09 (0.68)	4.53 (1.05)
$d(C_{10}\text{-OH})$	5.28 (0.63)	3.84 (0.53)	4.11 (0.47)
$d(H_{13}\text{-OH})$	6.20 (0.71)	6.02 (0.77)	4.43 (1.32)
$d(H_{10}\text{-OH})$	4.84 (0.85)	3.21 (0.92)	4.43 (0.82)

Table S3. Average $d(C_{13}/H_{13}\text{-OH})$ and $d(C_{10}/H_{10}\text{-OH})$ distances along the three calculated trajectories. Root mean square fluctuations are included in parentheses. Distances are given in Å.

In **Table S3** the calculated average distances: $d(C_{10}\text{-OH})$, $d(H_{10}\text{-OH})$, $d(C_{13}\text{-OH})$, and $d(H_{13}\text{-OH})$ are given for the three trajectories (TRJ1, TRJ2 and TRJ3). The results for TRJ1 and TRJ2 show that the $d(C_{10}/H_{10}\text{-OH})$ average distances are smaller than the $d(C_{13}/H_{13}\text{-OH})$ ones. Moreover, H_{10} seems to be, in average, better oriented for being abstracted than H_{13} This result would be in agreement with the experimental behavior as a 12-lipoxygenating enzyme (preference for H_{10} abstraction and oxygenation at C_{12}) of the Ile418Ala mutant of rabbit ALOX15. However, the results for TRJ3 seem to contradict the outcome of the two other trajectories because the $d(H_{13}\text{-OH})$ and $d(H_{10}\text{-OH})$ average distances turn out to be equal. In a study by some of us **(27)** on the AA binding to WT ALOX15, the $d(C_{10}/H_{10}\text{-OH})$ average distances obtained from MD trajectories were comparable to or even shorter than the $d(C_{13}/H_{13}\text{-OH})$ ones, in apparent contradiction to the experimental preference for H_{13} abstraction of WT ALOX15. All together, our simulations suggest that C_{10} and C_{13} are not really in such structurally different locations in a great number of the generated configurations for WT ALOX15-AA, neither for its Ile418Ala mutant. In fact, both carbon atoms can be simultaneously located close enough to the OH group for the corresponding H-abstraction processes being plausible. Remarkably, though, the difference [$d(C_{13}\text{-OH})$ - $d(C_{10}\text{-OH})$] moves to clearly greater values (C_{13}/H_{13} are farther away from the OH group with respect to C_{10}/H_{10}) in the Michaelis complex of the Ile418Ala ALOX15-AA mutant when compared to the WT ALOX15-AA one.

Geometric parameter	Ile418Ala rabbit ALOX15			Wildtype rabbit ALOX15		
Trajectory	TRJ 1	TRJ 2	TRJ 3	TRJ 1	TRJ 2	TRJ 3
$d(C_{20}\text{-C}\alpha\text{-A/I418})$	5.23 (1.02)	5.15 (0.39)	7.15 (1.81)	13.42 (1.11)	7.45 (0.90)	7.75 (0.76)
$d(C_{20}\text{-CO-A/I418})$	5.03 (1.05)	5.33 (0.61)	7.14 (1.93)	13.20 (1.20)	7.61 (0.95)	7.57 (0.77)

Table S4. Geometric parameters for arachidonic acid alignment at the active site of wildtype ALOX15 and its Ile418Ala mutant. Root mean square fluctuations are included in parentheses. Distances are given in Å.

In **Table S4** it is shown that the C20–C_α/CO-Ala/Ile418 distances are always smaller in the mutant when compared with the wild type enzyme (classified according to the different trajectories, that is, for different groups of structures).

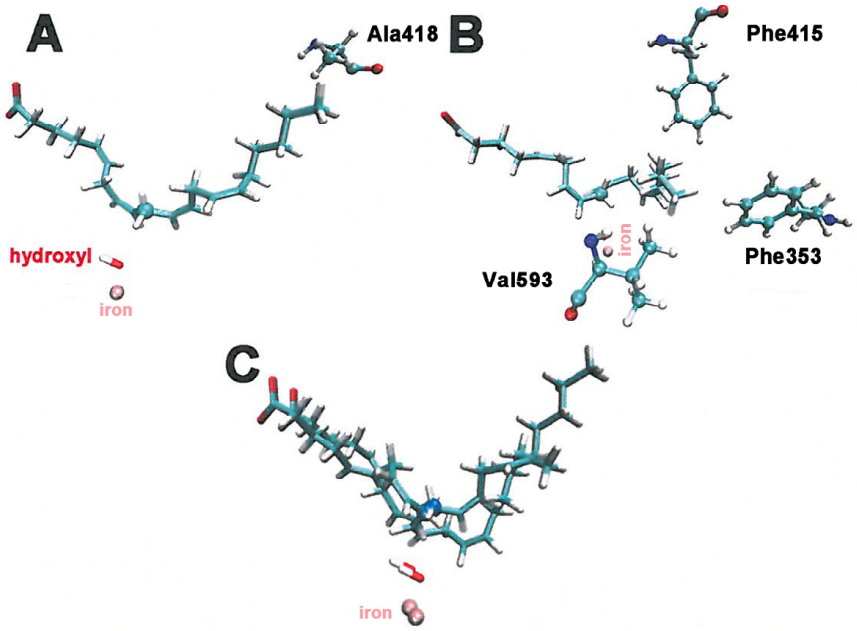

Figure S7. Two snapshots of Ile418Ala ALOX15-AA extracted from the set of reactive structures for H_{10}-abstraction of an MD trajectory of the *in silico* model. A) Reactive structure with the AA methyl end close to the Ala418 residue; B) Reactive structure with the AA methyl end interacting with the hydrophobic residues Phe415, Phe353 and Val594; C) Overlay of the AA structures shown in A) and B.

In **Figure S7** two other representative reactive structures of the mutant are depicted to illustrate that the fatty acid tail is interacting with Ala418 (**Figure S7A**) but also with other hydrophobic active site residues such as Phe415, Phe353 and Val594 (**Figure S7B**) being C_{10} at the same position with respect to the OH group in both structures (**Figure S7C**).

Arachidonic acid is aligned at the active site of the wildtype rabbit ALOX15 in such a way that proS- hydrogen at C10 is localized in a distance of 2.97 Å from the iron-bound hydroxyl group. In contrast, for the 12-lipoxygenating Ile418Ala mutant this distance is decreased to 2.51 Å, which represents a better alignment for 12-lipoxygenation **(Figure S8)**.

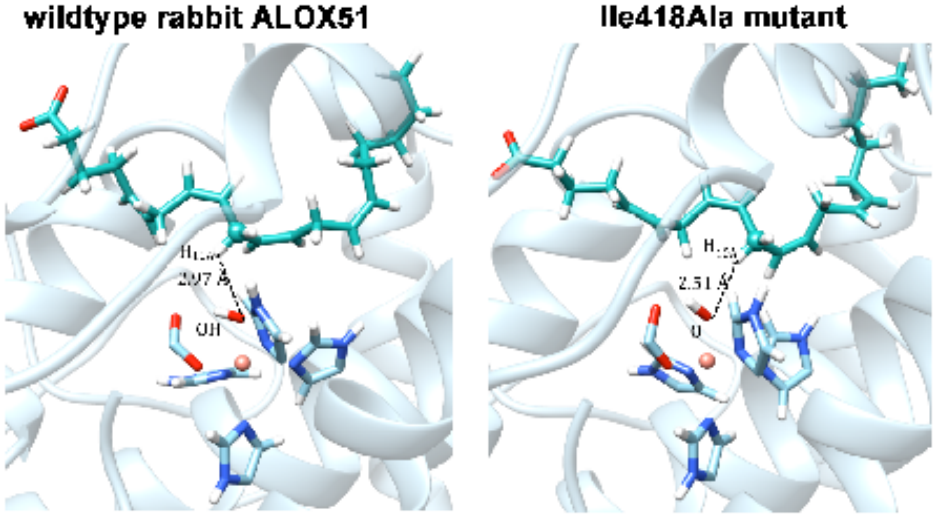

Figure S8. Arachidonic acid alignment at the active site of wildtype rabbit ALOX15 and its Ile418Ala mutant.

Table S5. Main geometric parameters of reactants and TSs of H_{10} and H_{13} abstractions. Distances are given in Å.

Structure	atom	d(H_{10}-OH)		d(C_{10}-H_{10})		d(C_{10}-OH)		∠(C-H_{10}-O)		∠(H_{10}-O-H)	
		R	TS	R	TS	R	TS	R	TS	R	TS
I	H_{10}	2.79	1.36	1.10	1.28	3.44	2.62	117.8	165.2	81.5	94.5
II	H_{10}	2.67	1.36	1.10	1.28	3.51	2.62	133.2	166.7	74.3	94.1
III	H_{10}	2.70	1.35	1.10	1.28	3.28	2.63	112.4	176.2	75.4	100.5
IV	H_{10}	2.63	1.37	1.10	1.26	3.29	2.63	117.7	173.3	81.5	99.4
V	H_{10}	3.17	1.36	1.10	1.28	3.47	2.63	96.6	173.7	62.0	97.8
VI	H_{10}	2.57	1.30	1.09	1.35	3.66	2.64	172.0	172.0	98.2	103.7
VII	H_{10}	2.60	1.30	1.09	1.34	3.67	2.63	162.9	173.4	89.1	103.0
VIII	H_{10}	2.58	1.29	1.10	1.33	3.63	2.61	162.0	172.3	91.9	100.9
IX	H_{10}	2.43	1.31	1.10	1.30	3.52	2.61	171.6	176.4	87.5	97.8
X	H_{10}	2.54	1.30	1.10	1.32	3.59	2.62	160.0	174.7	95.4	97.2

Structure	atom	d(H_{13}-OH)		d(C_{13}-H_{13})		d(C_{13}-OH)		∠(C-H_{13}-O)		∠(H_{13}-O-H)	
		R	TS	R	TS	R	TS	R	TS	R	TS
XI	H_{13}	2.47	1.33	1.10	1.31	3.42	2.63	145.0	172.1	108.8	105.0
XII	H_{13}	2.98	1.33	1.10	1.31	3.91	2.64	143.5	175.7	99.9	105.7
XIII	H_{13}	2.22	1.34	1.10	1.30	3.31	2.63	171.0	172.3	101.4	103.0
XIV	H_{13}	2.46	1.36	1.10	1.30	3.53	2.65	161.6	169.7	111.0	105.6
XV	H_{13}	2.64	1.36	1.10	1.29	3.73	2.65	175.2	174.1	106.2	104.6
XVI	H_{13}	2.38	1.32	1.10	1.32	3.45	2.64	162.3	173.6	120.4	107.1
XVII	H_{13}	2.41	1.34	1.10	1.30	3.50	2.64	171.0	175.5	102.4	105.3
XVIII	H_{13}	2.75	1.35	1.10	1.30	3.83	2.64	169.1	171.9	107.1	105.3
XIX	H_{13}	2.40	1.34	1.10	1.31	3.48	2.65	166.2	174.4	112.3	107.4
XX	H_{13}	2.41	1.32	1.10	1.31	3.48	2.63	162.8	172.6	96.1	103.0

In **Table S5** the most relevant interatomic distances of the selected structures at the reactant minima and at the transition states of the calculated H-abstraction potential energy profiles are given.

Evaluation of the geometric data obtained for the enzyme substrate complexes indicated that the distance calculations do not correlate with the functional enzyme properties. In fact, among the possible structures obtained for wildtype rabbit ALOX15 we found structures, which are clearly susceptible for major 12-lipoxygenation. Thus, the geometry of the enzyme-substrate may not be considered the major structural basis of the triad concept. Thus we calculated the energy barriers for the formation of the enzyme substrate complexes. In **Table S6** the calculated potential energy barriers for the transition states derived from the Michaelis complexes for structures I-X (suitable for 12-lipoxygenation) and XI-XX (suitable for 15-lipoxygenation) are presented. The energy barriers calculated for C13-hydrogen abstraction (15-lipoxygenation) ranged from 64 to 91 kJ/mol. In contrast, for C10-hydrogen abstraction (12-lipoxygenation) the energy barriers varied between 53 to 125 kJ/mol. To explore whether 12- or 15-lipoxygenation is preferentially catalyzed by the Ile418Ala mutant, the exponential average potential energy barriers for H10- and H13- abstractions were calculated. Here we found an exponential average potential energy barrier of 59 kJ/mol for H10-abstraction but 69 kJ/mol for H13-abstraction at 300 K. The 10 kJ/mol higher

energy barrier for the transition state of 15-lipoxygenation is consistent with the experimental observation of preferential 12-lipoxygenation of the Ile418Ala mutant of rabbit ALOX15.

Structure	Hydrogen abstraction from	Energy barrier kJ/mol)	Structure	Hydrogen abstraction from	Energy barrier (kJ/mol)
I	C_{10}	70.29	XI	C_{13}	88.66
II	C_{10}	73.22	XII	C_{13}	91.04
III	C_{10}	61.21	XIII	C_{13}	64.06
IV	C_{10}	53.39	XIV	C_{13}	68.12
V	C_{10}	74.43	XV	C_{13}	82.59
VI	C_{10}	125.23	XVI	C_{13}	78.70
VII	C_{10}	106.06	XVII	C_{13}	71.13
VIII	C_{10}	112.09	XVIII	C_{13}	74.98
IX	C_{10}	86.27	XIX	C_{13}	84.64
X	C_{10}	100.25	XX	C_{13}	73.72
Exponential average	**C_{10}**	**58.99**	**Exponential average**	**C_{13}**	**69.04**

Table S6. Potential energy barriers (kJ/mol) for 12-lipoxygenation (C_{10} hydrogen abstraction) and 15-lipoxygenation (C_{13}-hydrogen abstractions) by rabbit ALOX15 and its Ile418Ala mutant.

References

1. Jisaka M, Kim RB, Boeglin WE, & Brash AR (2000) Identification of amino acid determinants of the positional specificity of mouse 8S-lipoxygenase and human 15S-lipoxygenase-2. *The Journal of biological chemistry* 275(2):1287-1293.
2. Saura P, Suardíaz R, Masgrau L, Lluch JM, & González-Lafont À (2014) Unraveling How Enzymes Can Use Bulky Residues To Drive Site-Selective C–H Activation: The Case of Mammalian Lipoxygenases Catalyzing Arachidonic Acid Oxidation. *ACS Catalysis*:4351-4363.
3. Humphrey W, Dalke A, & Schulten K (1996) VMD: visual molecular dynamics. *Journal of molecular graphics* 14(1):33-38, 27-38.
4. Hoover WG (1985) Canonical dynamics: Equilibrium phase-space distributions. *Physical review. A* 31(3):1695-1697.
5. Ryckaert J, Ciccotti G, & Berendsen H (1977) Numerical-integration of cartesian equations of motion of a system with contraints - molecular dynamics of n-alkanes. *J. Comput. Phys.* 23(3):327-341.
6. Brooks BR*, et al.* (2009) CHARMM: the biomolecular simulation program. *Journal of computational chemistry* 30(10):1545-1614.
7. Brooks BR*, et al.* (1983) CHARMM - a program for macromolecular energy minimization and dynamics calculations. *J. Comput. Chem.* 4(2):187-217.
8. Feller S, Gawrisch K, & MacKerell A (2001) Polyunsaturated Fatty Acids in Lipid Bilayers: Intrinsic and Environmental Contributions to Their Unique Physical Properties. *Journal of the American Chemical Society* 124(2):318-326.
9. Feller S & MacKerell A (2000) An Improved Empirical Potential Energy Function for Molecular Simulations of Phospholipids. *The Journal of Physical Chemistry B* 104(31):7510-7515.

10. MacKerell AD*, et al.* (1998) All-atom empirical potential for molecular modeling and dynamics studies of proteins. *J Phys Chem B* 102(18):3586-3616.
11. Mackerell AD, Jr., Feig M, & Brooks CL, 3rd (2004) Extending the treatment of backbone energetics in protein force fields: limitations of gas-phase quantum mechanics in reproducing protein conformational distributions in molecular dynamics simulations. *Journal of computational chemistry* 25(11):1400-1415.
12. Saam J, Ivanov I, Walther M, Holzhutter HG, & Kuhn H (2007) Molecular dioxygen enters the active site of 12/15-lipoxygenase via dynamic oxygen access channels. *Proceedings of the National Academy of Sciences of the United States of America* 104(33):13319-13324.
13. Sherwood P*, et al.* (2003) QUASI: A general purpose implementation of the QM/MM approach and its application to problems in catalysis. *Theochem-J. Mol. Struct.* 632:1-28.
14. Ahlrichs R, Bar M, Haser M, Horn H, & Kolmel C (1989) Electronic-structure calculations on workstation computers - the program system turbomole. *Chem. Phys. Lett.* 162(3):165-169.
15. Smith W & Forester T (1996) DL_POLY_2.0: A general-purpose parallel molecular dynamics simulation package. *J. Mol. Graph.* 14(3):136-141.
16. Bakowies D & Thiel W (1996) Hybrid Models for Combined Quantum Mechanical and Molecular Mechanical Approaches. *The Journal of Physical Chemistry B* 100(25):10580-10594.
17. de Vries AH*, et al.* (1999) Zeolite Structure and Reactivity by Combined Quantum-Chemical−Classical Calculations. *The Journal of Physical Chemistry B* 103(29):6133-6141.
18. Liu D & Nocedal J (1989) On the limited memory bfgs method for large-scale optimization. *Math. Program.* 45(3):503-528.
19. Nocedal J (1980) Updating quasi-newton matrices with limited storage. *Math. Comput.* 35(151):773-782.
20. Baker J (1986) An algorithm for the location of transition-states. *J. Comput. Chem.* 7(4):385-395.
21. Banerjee A, Adams N, Simons J, & Shepard R (1985) Search for stationary-points on surface. *J. Phys. Chem.* 89(1):52-57.
22. Billeter S, Turner A, & Thiel W (2000) Linear scaling geometry optimisation and transition state search in hybrid delocalised internal coordinates. *PCCP Phys. Chem. Chem. Phys.* 2(10):2177-2186.
23. Becke A (1993) Density-functional thermochemistry .3. The role of exact exchange. *J. Chem. Phys.* 98(7):5648-5652.
24. Harihara P & Pople J (1973) Influence of polarization functions on molecular-orbital hydrogenation energies. *Theor. Chim. Acta* 28(3):213-222.
25. Hay P & Wadt W (1985) Abinitio effective core potentials for molecular calculations - potentials for the transition-metal atoms sc to hg. *J. Chem. Phys.* 82(1):270-283.
26. Lonsdale R & Mulholland AJ (2014) QM/MM modelling of drug-metabolizing enzymes. *Curr Top Med Chem* 14(11):1339-1347.
27. Toledo L, Masgrau L, Maréchal JD, Lluch JM, & González-Lafont A (2010) Insights into the mechanism of binding of arachidonic acid to mammalian 15-lipoxygenases. *J Phys Chem B* 114(20):7037-7046.